

Precision interferometric dilatometer

E. G. Wolff and R. C. Savedra

Citation: *Rev. Sci. Instrum.* **56**, 1313 (1985); doi: 10.1063/1.1137997

View online: <http://dx.doi.org/10.1063/1.1137997>

View Table of Contents: <http://rsi.aip.org/resource/1/RSINAK/v56/i7>

Published by the [American Institute of Physics](#).

Related Articles

Continuously tunable optical multidimensional Fourier-transform spectrometer
Rev. Sci. Instrum. **84**, 023107 (2013)

The frequency stabilization method of laser feedback interferometer based on external cavity modulation
Rev. Sci. Instrum. **84**, 025108 (2013)

Efficient end-fire coupling of surface plasmons on flat metal surfaces for improved plasmonic Mach-Zehnder interferometer
J. Appl. Phys. **113**, 053101 (2013)

Automation of an "Aculight" continuous-wave optical parametric oscillator
Rev. Sci. Instrum. **84**, 013102 (2013)

Two-path solid-state interferometry using ultra-subwavelength two-dimensional plasmonic waves
Appl. Phys. Lett. **102**, 021104 (2013)

Additional information on *Rev. Sci. Instrum.*

Journal Homepage: <http://rsi.aip.org>

Journal Information: http://rsi.aip.org/about/about_the_journal

Top downloads: http://rsi.aip.org/features/most_downloaded

Information for Authors: <http://rsi.aip.org/authors>

ADVERTISEMENT

JANIS Does your research require low temperatures? Contact Janis today.
Our engineers will assist you in choosing the best system for your application.



10 mK to 800 K LHe/LN₂ Cryostats
Cryocoolers Magnet Systems
Dilution Refrigerator Systems
Micro-manipulated Probe Stations

sales@janis.com www.janis.com
Click to view our product web page.

Precision interferometric dilatometer

E. G. Wolff and R. C. Savedra

Materials Sciences Laboratory, The Aerospace Corporation, El Segundo, California 90245

(Received 1 October 1984; accepted for publication 20 March 1985)

An improved double Michelson laser interferometer dilatometer is described. The unit is suitable for the study of materials of arbitrary size or shape with time-dependent and near zero coefficients of thermal expansion (CTE) over the range 100 to > 450 K. Direct recording of four amplified photodetector signals gives a $\Delta L/L$ resolution of 5×10^{-8} and an average CTE error in the 10^{-10} – 10^{-9} K^{-1} range. An inexpensive automatic digital counter–microprocessor combination permits recording of instantaneous $\Delta L/L$ and CTE values at > 30 -s intervals. The resolution of $\Delta L/L$ in this case is $< 8 \times 10^{-7}$ while the instantaneous CTE (4 K interval) has an uncertainty of $< 2 \times 10^{-7} \text{ K}^{-1}$. The latter values are based on a counting unit of $\lambda/2$ and interpolating. Smaller counting units reduce errors proportionately to the system noise level and the limitations of the temperature measurement.

INTRODUCTION

Michelson interferometry is widely used to detect small, even subangstrom, displacements^{1–3} (e.g., in piezoelectric transducer calibration⁴), but has seen limited application in the measurement of thermally induced expansions. Earlier methods were subject to complexity, differential techniques, nonuniform temperature gradients, and/or expense.^{5–7} A double Michelson interferometer was developed³ that is capable of measuring coefficients of thermal expansion (CTEs) of arbitrarily shaped samples, ranging in temperature from 100 to 450 K to a resolution of $< 10^{-8} \text{ K}^{-1}$.

The large number of optics components (over 30) required lengthy alignment procedures and special features were needed to accommodate temperature effects on the optics. Since both interferometers were actually *in vacuo*, a complex remote beam steering device would be needed to account for sample movements during an experiment. (Problems with this approach are outlined by Drotning.⁷) In subsequent work some advantages of phase modulation over polarization effects for automated signal processing were explored.^{8,9} In the latter system, the harmonics of the modulated fringe pattern, detected by a single photodetector, are compared to generate the required phase information. Drawbacks included a requirement of > 1 kHz modulation frequency to achieve adequate immunity from sample vibration induced noise. This in turn required piezoelectric transducers (PZTs) to operate at their resonant frequencies for adequate depth of modulation.

This report describes improvements in both the optics and signal processing of such an interferometer with major objectives being reductions in cost and set-up time, and an increase in ease of operation. A new data-reduction feature is time information, in recognition of the fact that measurement of low thermal expansion values can be significantly modified by the samples' finite thermal diffusivity and internal stress-relaxation mechanisms (such as microcracking or plastic flow in composite materials).

I. DILATOMETER DESCRIPTION

A. Optics

Figure 1 illustrates the basic features of a double Michelson interferometer. The optics were simplified from those described in Ref. 3 by bringing the beam splitters (B_1 and B_2) and sample-beam steering mirrors (P_1 and P_2) outside the vacuum system to allow rapid signal adjustments should the sample move. The optics components inside the vacuum chamber are limited to the reference mirrors (M_1 and M_2) and sample reflections (S_1 and S_2). If we denote the left-hand side interferometer as 1 in Fig. 1, and the other as 2, it is seen that the optical path length differences (OPLD) are given by

$$\text{OPLD}_1 = 2(B_1M_1 - B_1P_1S_1), \quad (1)$$

$$\text{OPLD}_2 = 2(B_2M_2 - B_2P_2S_2). \quad (2)$$

The factor of 2 comes from the fact that the optical path is twice the geometrical path. By symmetry

$$B_1M_1 + L_u + M_2B_2 = P_1S_1 + L_s + S_2P_2, \quad (3)$$

and

$$B_1P_1 = B_2P_2. \quad (4)$$

Adding the two OPLD, substituting B_1M_1 from Eq. (3) and using Eq. (4) gives

$$L_s = \frac{\text{OPLD}_1 + \text{OPLD}_2}{2} + L_u + 2(P_1B_1), \quad (5)$$

L_s and L_u are the sample length and width of the reference mirrors $M_1 - M_2$, respectively. The use of reflective mirrors, such as ULE (Corning Code 7971 ultralow expansion glass), on the ends of the sample increases L_s to $(L_0 + L_1 + L_2)$.

Accurate measurement of a change in sample length requires a zero or known length change in L_u and B_1P_1 . The first is accomplished by mounting the reference mirrors on a ULE glass or Zerodur block in a thermally insulated part of

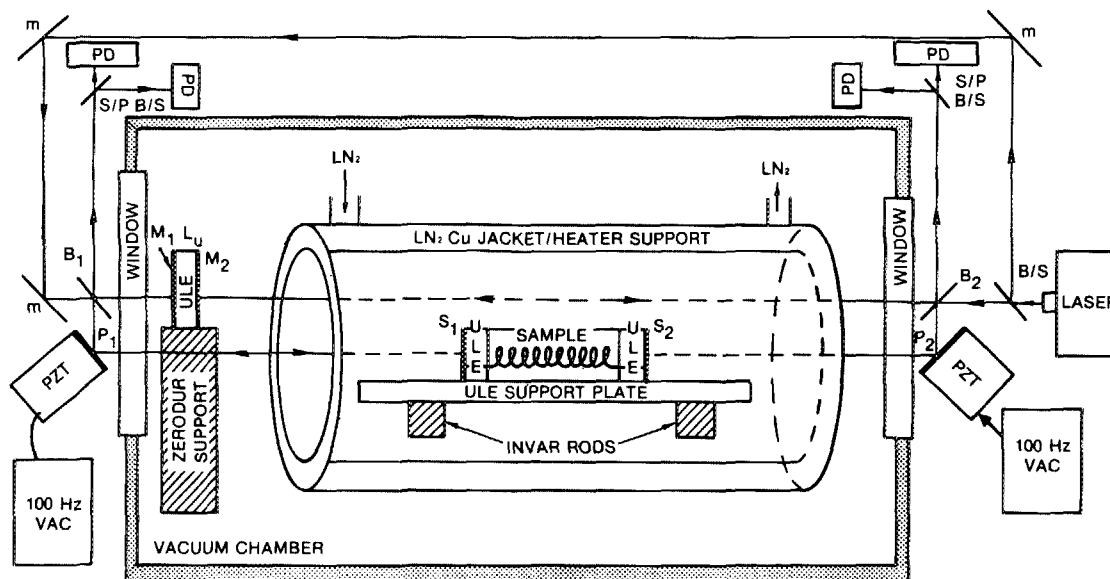


FIG. 1. Diagram of the double Michelson interferometer optics.

the system. Since the B_1P_1 (or B_2P_2) paths are in air, mounting must compensate for index of refraction changes (see Sec. I C). Sample end movement may be caused by the bowing of an unsymmetrical laminate. In this case, short focal length lenses³ are symmetrically positioned (for equal heat effects) to focus the beams on both sample and reference-mirror surfaces. Preferably, the normal dispersion of a single-frequency He-Ne laser beam can be modified with lenses or collimators to achieve focus on the sample ends without the need for lenses in the vacuum chamber.

B. Sample support

The sample support system required to maintain the axis of the sample parallel to the laser beams between the PZT mirrors (Fig. 1) has been described.^{3,10} The end faces of the sample must be flat and perpendicular to this axis to within a few tenths of a degree. They are polished and coated with a thin layer of Al, Au, or Cr. ULE glass end mirrors for porous samples are spring loaded, as cements tend to shift the mirrors. The apparatus of Fig. 1 handles samples of any size, with laser beam spacing, spot size, and uniform temperature being limitations. Modifications for larger samples have been described elsewhere.^{2,11} Temperature measurement is accomplished with two 2-mil Cu-Constantan thermocouples. They must be loosely positioned to prevent them from moving small samples during heating and cooling.

C. Error analysis

The rectangular beam arrangement in Fig. 1 provides immunity from errors resulting from uniform support table contraction and expansion. If the beams S_1P_1 and M_1B_1 are not quite parallel, errors are still small. For example, if the beam strikes one sample end 2.5 mm away from the parallel beam point, and the (steel) table heats or cools 5 °C during an experiment, the net measurement error is about 5 Å. Index-of-refraction changes in the vacuum chamber are negligible

if a diffusion pump is used. Drift is caused by room-temperature changes in the external optics. The major source of error is the air paths B_1P_1 and B_2P_2 . The temperature-induced change in optical path length (OPL) is

$$\Delta \text{OPL} = 2\Delta T(\partial B_1P_1/\partial T) = 2\Delta T[\alpha l_a + (\partial n/\partial T)l_b], \quad (6)$$

where l_a and l_b represent the mechanical connections and air distances, respectively, and α the CTE of the total support system. The largest term is $\partial n/\partial T$ of air, about $-9.33 \times 10^{-7} \text{ K}^{-1}$ in the vicinity of 22 °C, 50% RH and 1000 mb.¹² If $l_b = 12 \text{ mm}$, and $l_a = 25 \text{ mm}$, then α should be $\sim 4.5 \times 10^{-7} \text{ K}^{-1}$ for a zero error. A fused-silica support is suggested. With a Zerodur support (lower α) a typical drift rate of $\lambda/20 \text{ h}^{-1}$ is encountered in a room that fluctuates by 3 to 4 °C/day. For more precise work, these components (B and P) can be moved into the vacuum chamber.

The reference mirror support (e.g., Zerodur) is shielded from temperature excursion and a conservative error is

$$\begin{aligned} \Delta L_u &= \alpha L_u \Delta T = (1 \times 10^{-7}) (3 \times 10^{-3} \text{ m}) \quad (5) \\ &= 15 \times 10^{-10} \text{ m} \quad (15 \text{ \AA}). \end{aligned} \quad (7)$$

Temperature gradients in the support table could cause bowing and a change of B_1B_2 relative to P_1P_2 .^{2,3} This error, equivalent to ΔL_u in Eq. (3), has been transferred from the Zerodur plate in the vacuum chamber to the external optical bench. The error is kept negligible by insulating the heater/cooler from this bench and minimizing the beam separation (e.g., 10 mm) in Fig. 1. Lenses introduce errors if they change temperature (typically 100 Å for each degree K change).³ Temperature gradients in the sample cause errors in two ways: (a) by giving a false average temperature reading (with thermocouples) and (b) by distorting the end faces. Figure 2 illustrates the temperature difference between the surface and center of typical test samples as a function of heating/cooling rates. At a typical 2 °C/min rate, errors are ~ 0.1 °C. The sample end faces will become parabolic, and the position of the beam determines the relative error. It can be shown

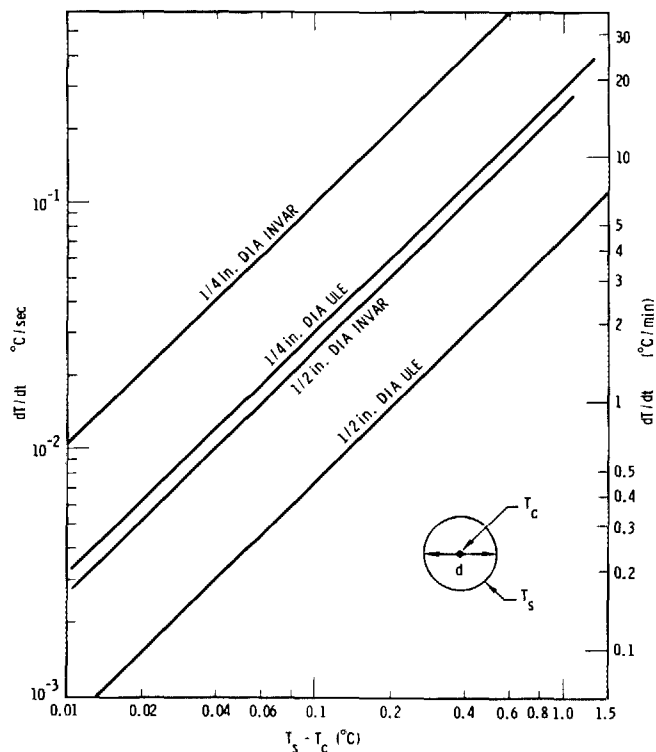


FIG. 2. Variation of radial ΔT with heating and cooling rate.

that this error is a maximum of $\sim \alpha_s \Delta T / 3$, where α_s is the sample CTE and ΔT is found from Fig. 2.

D. Operational procedure

The general procedure for maximizing the signal-to-noise ratio is as follows: The main laser beams are first aligned without the sample or the PZT mirrors, so that the back reflections are close to, but not into, the beam laser exit cavity. This involves adjusting the first beam-splitter position. The sample is inserted with the (heater/cooler removed) and the main beam is checked so that it clears the sample. The two beams over the sample are checked for overlap while the reference mirrors are temporarily removed. The reference mirrors are reinserted and the PZT mirrors are adjusted so that the beams B_1, B_2 and P_1, P_2 are parallel (with the sample in place). The sample orientation is adjusted by means of the horizontal Invar rods so that a fringe pattern above either beam splitter (B_1 or B_2) is obtained; the other side should then require minimal adjustments. The photodetectors are then inserted and final adjustments are made, using the oscilloscope signals to maximize the ellipse or circle pattern.

II. SIGNAL PROCESSING

The purpose of the signal processing electronics is to convert the irradiance distribution changes of the fringe patterns of the two interferometers into an analog signal proportional to the sample length change. The signal processing must recognize that the same fringe pattern changes occur whether the sample end faces move towards or away from the beam splitter, and that each end face can move in either

direction as a result of combined dilatational and translational sample motions. (Vibration in the sample support system is a major cause of translation, especially for small samples.) Polarization⁶ and phase modulation⁹ techniques are commonly used; here we outline a basic approach based on polarization monitoring and introduce a related technique based on scanning and digital counting. The electronics for this technique are presented in detail in Sec. III while the application to thermal expansion testing is illustrated in Sec. IV.

The fringe patterns are initially analyzed with S/P beam splitters and silicon photodiodes (Figs. 1 and 3). The PhotopTM UDT-455 detector/amplifier system (Silicon Photodiode Corp.) produces a voltage output that is typically ± 5 V with a good reflection and a 0.5-mW single-frequency He-Ne laser. This signal can be monitored in two ways: with either a dc or an ac approach, and in both cases the photodiode signals are applied to the x - y inputs of two oscilloscopes. A $\lambda/2$ fringe translation produces a 360° trace that is usually elliptical and can be adjusted with $\lambda/4$ plates. In the dc approach, either signal from each interferometer is plotted directly on a strip-chart recorder. A third pen is used to record temperature.

Air is briefly introduced into the vacuum chamber and the direction of signal motion around the ellipse on the scope is recorded and correlated with the strip chart motion. An increase in the index of refraction is equivalent to an increase in the longer arm of each interferometer. This is equivalent, in turn, to reducing the shorter arm if " n " remains constant, and this establishes the direction of motion on each sample end face. This method allows for continuous tracking of very weak signals, the limit being determined by sample vibrations caused by the mechanical vacuum pump.

The major drawback is that readjustment of the optics after a signal is lost may switch the polarizations and hence the apparent direction of sample movement. The signals are also unsuitable for automatic data processing. Continuous analysis of all four photodetector signals would yield sample expansion data only if the signal amplitude were constant (which is rarely the case because of the small sample motions involved). Nevertheless, this method allows an operator to extract all the needed phase information after the experiment from the sinusoidal traces on the chart.

An ac method was developed that requires only that the operator occasionally adjust the optics to maintain a minimum ellipse size on the oscilloscopes. This minimum size depends on the signal-to-noise ratio (which is related to sample reflectance, beam alignment, and sample vibrations). Below the minimum size, the counter (described below) starts skipping counts, a phenomenon that is detectable from a discontinuity on the strip chart recorder. A microprocessor can be readily programmed to correct for this discontinuity. The range of useful signal amplitudes varies typically from ± 5 V to a few mV. If a minimum signal cannot be regained by adjustment of the optics (e.g., mirrors B and P), it is possible to convert over to the dc system and the dc offset is adjusted manually.

In the ac method, the PZTs in Fig. 1 are oscillated at a total displacement of just under $\lambda/2$, so that an almost-

closed ellipse is displayed on each scope. A sawtooth rather than square wave input to the PZT is helpful. The frequency chosen (from 60 to 100 Hz) is based on a spectrum analysis of the mechanical system and represents a minimum extraneous noise region and an achievable PZT displacement. Direction of motion is determined by applying a dc voltage to each PZT and correlating changes in interferometer arm length.

The counting method is a scanning technique involving zero crossing detection and averaging for fringe interpolation. Advantages over phase-modulated techniques^{8,9} include simplified electronics and the use of interchangeable PZTs operating at low frequencies. This technique is sensitive only to gross shocks to the system that cause optical misalignment. Tuning of frequencies is unnecessary, as the fringe pattern is scanned in a manner duplicating the actual vibration-caused scanning. On the debit side, two photodetectors are still needed per interferometer and the state of polarization must be adjusted. Also, frequency response is lower, reducing one's ability to study simultaneous crack formation in materials.¹

III. AC COUNTER ELECTRONICS

Figure 3 illustrates schematically the automated ac counting system. This consists of (a) a signal conditioner (Fig. 4), (b) clippers (Fig. 5), and (c) quadrature counters with digital-to-analog (D/A) converters (Fig. 6). The latter provide data suitable for microprocessor analysis (see Sec. IV).

The signal conditioner consists of a three-stage signal-conditioning network. The photodetector output has both ac and dc components. The 22 μ F capacitor cancels out the dc level when switch "S" in Fig. 4 is closed, so that the ac components will be centered around ground. This is a high-pass filter that eliminates signals <0.5 Hz. The next stage is a noninverting variable-gain amplifier that sets the conditional signal at any desired level. This is followed by a third-order low-pass filter that cancels out all frequencies >1 kHz. It was found that if filtering about the modulator frequency is too narrow, some of the phase information in the x - y signals is distorted. The low-pass filter suppresses high-frequency noise spikes that interfere with the directional counters. There are additional possibilities for automatic gain control here. The purpose would be to keep the signal

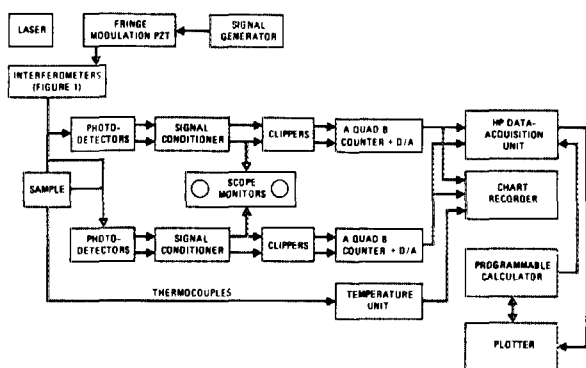


FIG. 3. Block diagram of the test setup for the interferometric dilatometer.

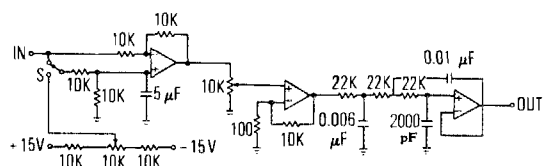


FIG. 4. Schematic of the signal conditioner ($\times 4$ for the double Michelson interferometer).

input to the digital counter within an optimum range between the clipper threshold level and the distortion limit for the operational amplifiers. A promising approach for use at low frequencies (~ 100 Hz) is with operational transconductance amplifiers (OTAs).

The clipper circuit in Fig. 5 converts the amplified filtered sine-wave signals to a fixed square-wave output having a value of 5 V max when the sine-wave input is above 0 V, and a 0 V output when the input drops below 0 V. The conditioner signals are first fed into a buffer amplifier and then clipped at 5 V by a Zener diode that interfaces with the logic gates. The square-wave signals are fed into Schmitt trigger NAND gates (#74132) for further waveform conditioning.

In the A quad B counter (Fig. 6), the square waves are time and phase analyzed by a series of one-shots and logic gates. The one-shots respond to the signal quadrant crossings by producing short pulses at the square-wave signal transitions. These pulses are directionally routed by the logic steering gates into the appropriate up or down counter inputs. With the aid of Boolean algebra¹³ in Fig. 7, it can be shown how the logic steering gates and one-shots function for different counting states. The circuit shows the letters A and B representing the clipped photodetector signals, and the letters C, D, E, and F representing the one-shot short pulse transition signals. Figure 8 shows that the one-shots respond to the two counting conditions that can occur. By substituting the logic level values for any time t into each appropriate letter of the output Boolean expression, one can determine the circuit output response at any given time. An evaluation of the two counting states in Table I shows how the final up and down outputs respond to the clockwise and counter-clockwise interferometer fringe signals (A and B). The direction of counting is determined by which clock input is pulsed with a low-to-high transition while the other clock input is high for the up/down counter.

The analog-to-digital (A/D) converter employs a 12-bit binary base and is used in a half full-scale output state. Thus, a total of output counts at half full scale is ± 1024 counts. With one fringe ($\lambda/2$) equaling 4 counts, the counting range is reduced to ± 256 fringes before reset.

The linearity of the counter output was tested by application of a known Δ OPLD. Figure 9 represents the counter

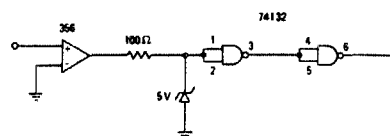


FIG. 5. Schematic of the clipper circuit.

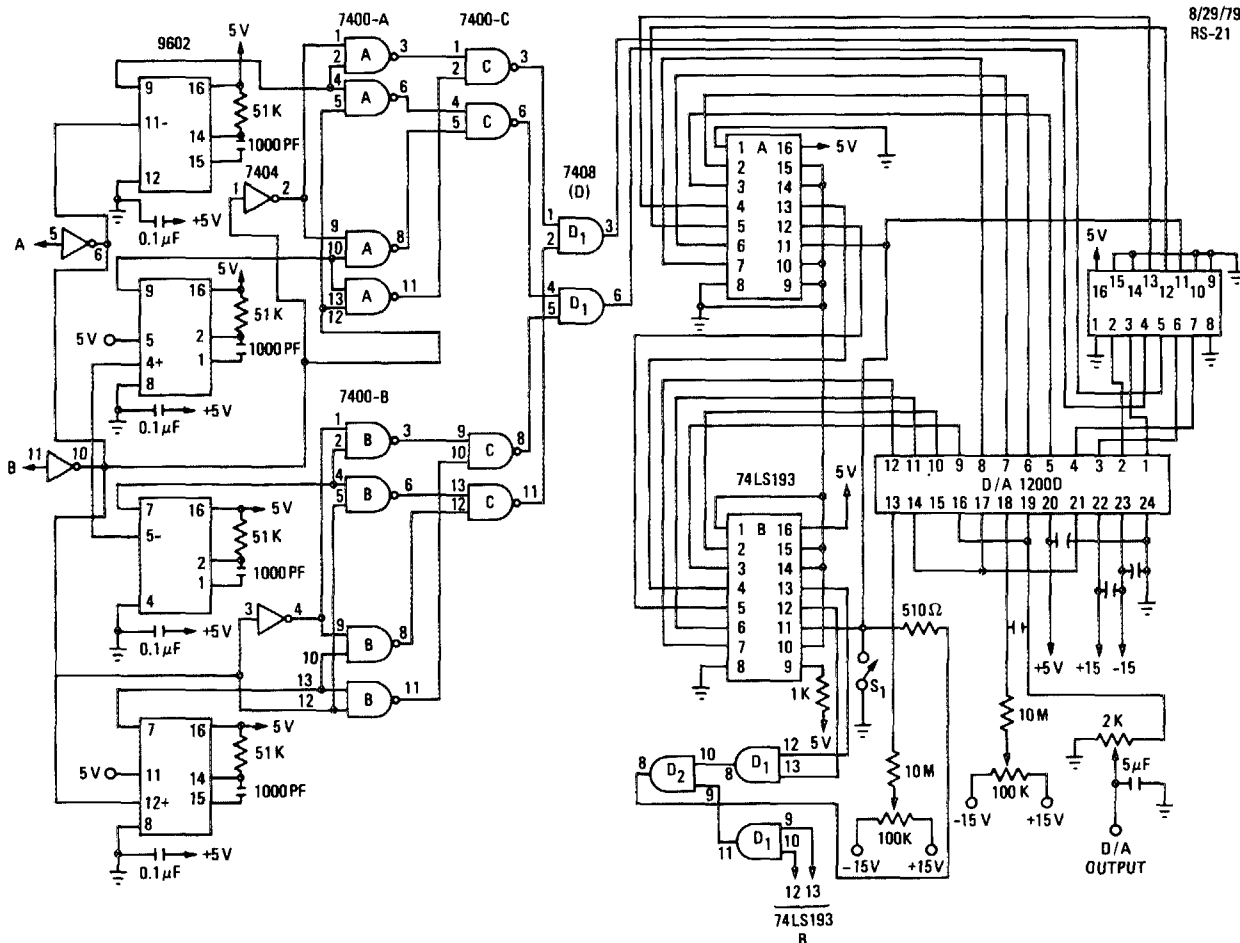


FIG. 6. Schematic of the A quad B counter and the D/A converter.

output when a mirror was placed against the window of one interferometer (Fig. 1) and a dc voltage was applied to the PZT (Burleigh PZ40). This moves the mirror P at $\sim 45^\circ$ to the sample beam. The counter was set at $10 \text{ mV} = \lambda / 2 = 3164 \text{ \AA}$ by calibration with 360° circle rotation on the scope. The change in optical path length difference (OPLD), proportional to the counter output, is given by

$$\Delta \text{OPLD}(\text{\AA}) = 2 \times 10^4 \phi V \sin \theta, \quad (7)$$

where ϕ is the PZT characteristic ($\sim 0.015 \mu\text{m/V}$) and θ the

beam incidence angle between the sample beam coming from the beam splitter and the surface of the mirror in the direction of mirror motion. The curve of Fig. 9 falls below the prediction of Eq. (7) due to PZT hysteresis and rate effects. Nevertheless, the curve shows that the counter can follow the (steady) motion to within $\pm 15 \text{ \AA}$. The maximum error of the D/A counter output is $\pm \frac{1}{4}$ bit for the three-digit BCD circuit, which is then $1/4$ of one count, $\lambda / 8$, or 791 \AA .

IV. DATA REDUCTION

Many techniques (e.g., Fizeau interferometry) used to determine thermal expansion coefficients require thermal equilibration of the system before a ΔL of the sample is re-

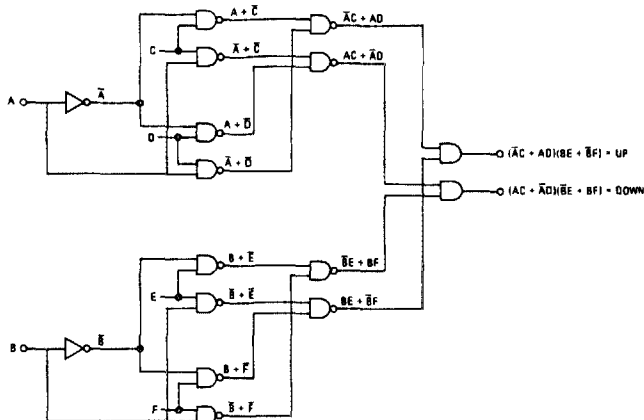


FIG. 7. Schematic of the steering logic circuit.

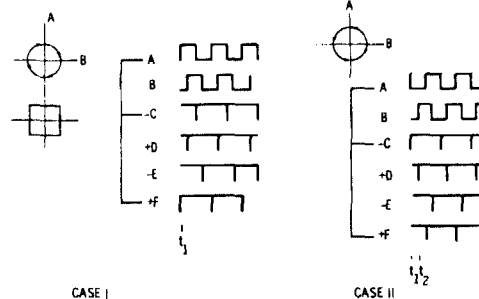


FIG. 8. Diagram of directional counting sequence.

TABLE I. Logic circuit evaluation.

Case I @ t_1		
A = 1	UP = $(\bar{A}C + AD)(BE + \bar{B}F)$	DOWN = $(AC + \bar{A}D)(\bar{B}E + BF)$
B = 0	= $(T \cdot 1 + 1 \cdot 1)(0 \cdot 1 + 0 \cdot 0)$	= $(1 \cdot 1 + 1 \cdot 1)(0 \cdot 1 + 0 \cdot 0)$
C = 1	= $(0 \cdot 1 + 1)(0 + 1 \cdot 0)$	= $(1 + 0 \cdot 1)(1 \cdot 1 + 0)$
D = 1	= $(0 + 1)(0 + 0)$	= $(1 + 0)(1 + 0)$
E = 1	= 1·0	= 1·1
	= 0	= 1
Case II @ t_2		
A = 0	UP = $(\bar{A}C + AD)(BE + \bar{B}F)$	DOWN = $(AC + \bar{A}D)(\bar{B}E + BF)$
B = 1	= $(0 \cdot 1 + 0 \cdot 0)(1 \cdot 1 + 1 \cdot 1)$	= $(0 \cdot 1 + 0 \cdot 0)(1 \cdot 1 + 1 \cdot 1)$
C = 1	= $9 \cdot 1 + 0(1 + 0 \cdot 1)$	= $(0 + 1 \cdot 0)(0 \cdot 1 + 1)$
D = 0	= $(1 + 0)(1 + 0)$	= $(0 + 0)(0 + 1)$
E = 1	= 1·1	= 0·1
	= 1	= 0

corded. Others, such as differential quartz dilatometers lack sufficient accuracy and resolution for many new ultralow expansion materials. In many cases, the thermal expansion characteristics are time dependent. Creep effects occur in composites¹¹ and viscoelastic materials. In spite of the fact that many low thermal conductivity samples may never reach thermal equilibrium in a CTE test (as Fig. 2 indicated), the expansion behavior should be correlated with both temperature and time. A method for recording ΔL , T , and t data in real time is outlined as follows. It is based on the Hewlett-Packard HPIL microprocessor system, although any similar real-time data-acquisition system would suffice.

The two interferometric counter outputs and analog temperature signals are sampled at predetermined intervals (e.g., by a timer module in the HP41CV component of the HPIL System). In this case, $\Delta L/L$ versus T points can be printed at ≥ 30 -s intervals. The instantaneous CTE is simultaneously determined by a regression analysis of the present and two prior $\Delta L/L$ values and plotting at the prior temperature. Color coding helps to differentiate the $\Delta L/L$ from CTE data. A program can also be written which will change the scale of either parameter as desired. Since the time spacing of the data points is known, deviations from smooth curves can be correlated with the heating or cooling rates.

The microprocessor may be also used to correct for counting errors caused by extreme line-voltage surges, mechanical shocks, or very low signal-to-noise ratios (when optics realignment is indicated). For example, a critical voltage is set in the calculator program. If a reading exceeds the previous one by this value, the program discards that reading and plots instead an extrapolated one based on three (or

more) former readings. A linear regression analysis based on three or more prior $\Delta L/L$ readings is usually sufficient. Alternative approaches include power law curve fittings. These previous readings are then "shifted" to the level of the actual signal so that subsequent readings are unaffected. At the same time, this extrapolation gives an instantaneous CTE. The major problem with this approach is that some materials exhibit rapid changes in CTE (due to microcracking or plastic flow of the matrix, for example). Limited use of the correction mode is, therefore, recommended.

Figure 10 illustrates these features for a quartz rod that was first cooled from ambient temperature, then heated to ~ 400 K and cooled back to ambient. The main hysteresis is caused by thermal lag of the inside of the rod and is diminished by slower cooling rates. An initial setting of eight for the exponent for CTE proved too sensitive, and a switch to seven on heating improved the data display. (These values were plotted per individual data point; averaging over several data points permits use of the 8 scale.) (The occasional discontinuities in the $\Delta L/L$ curve are results without the corrections described above.) A wider range of instantaneous CTEs is recorded whenever the temperature trend is reversed or isothermal data are desired.

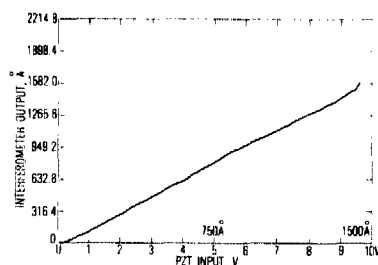


FIG. 9. Interferometric counter output vs voltage applied to PZT-driven mirror (1000 V \equiv 15 μ m motion).

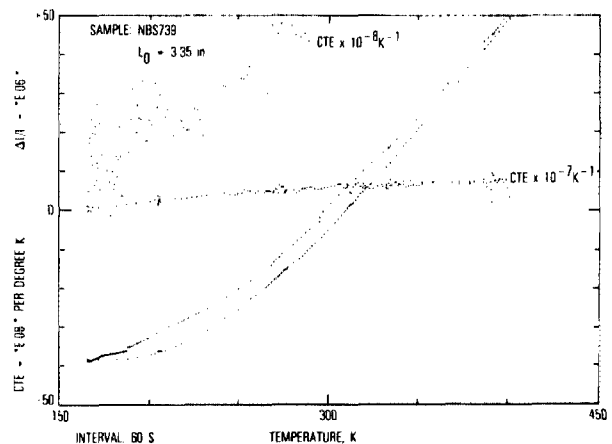


FIG. 10. Thermal strain cycle and instantaneous CTE vs temperature for a fused silica rod. The double curve represents 60-s interval readings of $\Delta L/L$ on a $\pm 50 \times 10^{-6}$ scale from 300 to 400 to 160 to 300 K. During the 160 to 300 K excursion, the CTE scale sensitivity was increased, from $\pm 50 \times 10^{-7}$ to $\pm 50 \times 10^{-8} \text{ K}^{-1}$.

V. DISCUSSION

The optical, signal-processing, and data-reduction systems of a precision double Michelson interferometer have been described. Real-time thermal strain and instantaneous CTEs can be measured for a sample of arbitrary size or shape for temperatures from 100 to > 450 K. An inexpensive signal processor permits data sampling at regular intervals, in order to present simultaneous time-dependent behavior.

Figure 9 indicated that fluctuations from a known continuous displacement can be followed by the electronic counting system to $\pm 15 \text{ \AA}$ (for one of the two interferometers). The absolute accuracy for each counting system is limited by the accuracy of the counter digital electronics where the BCD components are accurate to $\pm \frac{1}{4}$ bit, equivalent to $\lambda/8$ or 791 \AA . This represents the maximum deviation from any total excursion; that is, ΔL is known to be $\pm \lambda/8$ for the range $\lambda/2$ to the coherence length of the laser (assuming the counter is designed for that range). The unit of counting can, of course, be changed to any fraction of a fringe, so that the resolution of $\lambda/8$ is not an inherent limitation of the system.

A fundamental restriction is the noise level of the output of the individual photodetectors. The amplified photodetector signals can be recorded directly. Ref. 1, for example, illustrated typical signals from an interferometer of this type. The peak-to-peak voltage with the passage of half a fringe was readily amplified to 625 mV (corresponding to a $\lambda/4$ displacement). The superimposed electronic noise is caused mainly by sample vibration and is phase dependent. In our system, the maximum noise level was about $\pm 20 \text{ mV}$, suggesting a ΔL resolution of almost $\pm 20/625 \times (\lambda/4)$ or 51 \AA . Methods to reduce this value are available.¹ Since the CTE depends on temperature as well as on strain measurement, the thermocouple errors must be considered. Factors such as strain hardening, annealing, compositional variations, and thermal coupling to the sample tend to limit the accuracy of 2-mil Cu-Constantan thermocouples to about $\pm 0.5 \text{ }^\circ\text{C}$. This does not mean a random error, but rather an uncertainty in the end points over a typical temperature excursion, e.g., $200 \text{ }^\circ\text{C}$. The fractional error in CTE may then be computed from

$$\frac{\sigma(\text{CTE})}{\text{CTE}_{av}} = \left[\left(\frac{\sigma(\Delta T)}{\Delta T} \right)^2 + \left(\frac{\sigma(\Delta L)}{\Delta L} \right)^2 + \left(\frac{\sigma(L_0)}{L_0} \right)^2 \right]^{1/2}, \quad (8)$$

where σ represents the standard deviation or estimated error. Taking values of $\sigma(\Delta T) = 0.5$, $\Delta T = 200 \text{ }^\circ\text{C}$, $\sigma(\Delta L) = 791 \text{ \AA}$, $\Delta L = \sigma(L_0) = 100 \mu\text{in.} = 2.54 \times 10^4 \text{ \AA}$, and $L_0 = 4 \text{ in} = 10^9 \text{ \AA}$, the fractional error in CTE is 0.03. Use of the photodetector signals directly reduces $\sigma(\Delta L)$ to 51 \AA and $\sigma(\text{CTE})/\text{CTE}_{av}$ by a factor of about 10. In the latter case, the temperature uncertainty would be the major error. Since actual CTE_{av} would be $\Delta L/\Delta TL_0$ or $1.27 \times 10^{-7} \text{ }^\circ\text{C}^{-1}$ in this case, use of the counter would mean $\sigma(\text{CTE}) = 4 \times 10^{-9} \text{ K}^{-1}$. The photo-detector signals measured directly would lead to $\sigma(\text{CTE}) \sim 4 \times 10^{-10} \text{ K}^{-1}$. The instantaneous CTE error would be about 50 times more due to the reduced temperature interval (to 4 K).

Further improvements in accuracy and resolution could be achieved by using calibrated thermocouples, nonmechanical vacuum pumps to reduce vibration, optical isolators, line voltage stabilization to eliminate voltage spikes, and an athermalized support system for the BP paths in the optics.

ACKNOWLEDGMENT

The authors wish to acknowledge the help of W. H. Ditrach in the operation and testing of the interferometer.

- ¹E. G. Wolf, "Measurement techniques for low expansion materials," in *Materials and Processes—In Service Performance* (9th National SEMPE Technical Conference Proceedings) (Soc. for the Advancement of Material and Process Engineering, Azusa, CA, 1977), pp. 57–72.
- ²E. G. Wolff and S. A. Eselun, *Rev. Sci. Instrum.* **50**, 502 (1979).
- ³E. G. Wolff and S. A. Eselun, *Proc. SPIE* **192**, 204 (1979).
- ⁴L. E. Drain, J. H. Speake, and B. C. Moss, *SPIE Proceedings, Vol. 136* (SPIE, Bellingham, WA).
- ⁵A. P. Miller and A. Cezairliyan, *Thermal Expansion 6*, edited by I. D. Peggs (Plenum, New York, 1978), pp. 131–143.
- ⁶Y. Souche, R. Vergne, J. C. Cotillard, J. L. Porteseil, G. Roblin, and G. Nomarski, *8th International Thermal Expansion Symposium*, edited by T. A. Hahn, NBS, June 1981 (Plenum, New York, 1984).
- ⁷W. D. Drotning in *Thermal Expansion 7*, edited by D. C. Larsen, (Plenum, New York, 1982); also SANDIA Report No. SAND 83-0197, UC-37, May 1983.
- ⁸S. A. Eselun and E. G. Wolff, *ISA Trans.* **19**, 58 (1980).
- ⁹S. A. Eselun, R. C. Savedra, and E. G. Wolff, Air Force Space Division Report No. SD-TR-81-113, 18 December 1981.
- ¹⁰E. G. Wolff and S. A. Eselun, U.S. Patent No. 4 313 679 (February 1982).
- ¹¹E. G. Wolff, B. K. Min, and M. H. Kural, *J. Mater. Sci.* **24**, 1141 (1985).
- ¹²J. C. Owens, *Appl. Opt.* **6**, 57 (1967).
- ¹³R. J. Tocci, *Digital Systems* (Prentice Hall, Englewood Cliffs, NJ, 1977), Chap. 2.